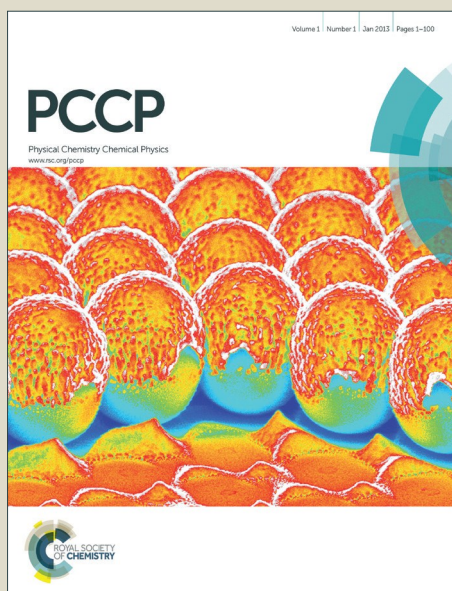


PCCP

Accepted Manuscript



This article can be cited before page numbers have been issued, to do this please use: B. Chen, V. Nguyen, J. C. S. Wu, R. Martin and K. Koí, *Phys. Chem. Chem. Phys.*, 2016, DOI: 10.1039/C5CP06999H.



This is an *Accepted Manuscript*, which has been through the Royal Society of Chemistry peer review process and has been accepted for publication.

Accepted Manuscripts are published online shortly after acceptance, before technical editing, formatting and proof reading. Using this free service, authors can make their results available to the community, in citable form, before we publish the edited article. We will replace this *Accepted Manuscript* with the edited and formatted *Advance Article* as soon as it is available.

You can find more information about *Accepted Manuscripts* in the [Information for Authors](#).

Please note that technical editing may introduce minor changes to the text and/or graphics, which may alter content. The journal's standard [Terms & Conditions](#) and the [Ethical guidelines](#) still apply. In no event shall the Royal Society of Chemistry be held responsible for any errors or omissions in this *Accepted Manuscript* or any consequences arising from the use of any information it contains.

1 Renewable fuel by photohydrogenation of CO₂: Impact of the
2 nature of Cu species loaded TiO₂

3 Bo-Ren Chen ¹, Van-Huy Nguyen ¹, Jeffrey C.S. Wu ^{1,*}, Reli Martin ², Kamila Kočí ²

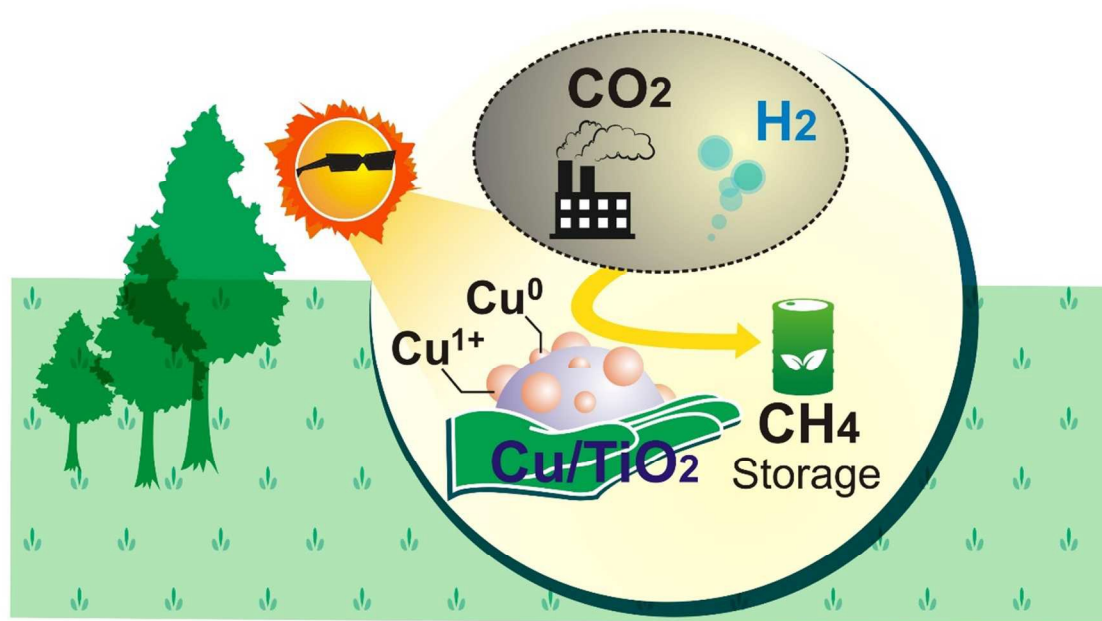
4 ¹ Department of Chemical Engineering, National Taiwan University, Taipei 10617, Taiwan

5 ² Institute of Environmental Technology, VŠB-Technical University of Ostrava, 17. listopadu
6 15/2172, Ostrava –Poruba 708 33, Czech Republic.

7 * Corresponding author

8 Phone: +886-2-23631994, Fax: +886-2-23623040, E-mail: cswu@ntu.edu.tw

9 Graphical abstract



- 10
- 11 Efficient gas-phase photocatalytic hydrogenation of CO_2 opens a feasible route not only to store
- 12 H_2 by converting into renewable fuel but also to cut down the atmospheric CO_2 greenhouse gas.

Abstract

Efficient gas-phase photocatalytic hydrogenation of CO₂ into desired fuel is achieved on Cu-loaded TiO₂ photocatalyst system. Firstly, the enhancing amount of Ti³⁺ rather than Ti⁴⁺ species in Cu-loaded TiO₂, in comparing with TiO₂ photocatalyst, provides an excellent opportunity to promote the photohydrogenation of CO₂. Additionally, the coexistence of Cu and Cu¹⁺ species during the photoreaction could also efficiently enhanced photocatalytic activity by prolonging the lifetime of electrons. To achieve the best photo-activity, the content of Cu species must be maintained at an appropriate low concentration ($\leq 1\text{wt.}\%$), and the corresponding highest CH₄ yield was 28.72 $\mu\text{mol g}^{-1}$. This approach opens a feasible route not only to store hydrogen converting into desired renewable fuel but also to cut down the atmospheric CO₂ greenhouse gas.

Keywords: photohydrogenation, carbon dioxide; renewable fuel, photocatalysis; Cu-loaded TiO₂

1. Introduction

Nowadays, hydrogen (H_2) is considered as energy for the future because of its clean energy, most abundant, flexible and highly efficient. Although the outlook will inevitably belong to H_2 , there are still growing concerns about the H_2 storage.^{1,2} In details, it requires 11,250 l to achieve 1 kg of H_2 under atmospheric pressure and room temperature. Even H_2 is compressed at 700 bars; its volumetric energy density is approximately six times lower than that of gasoline (8.8 kWh/l). Meanwhile, the volumetric energy density of natural gas, which mainly consists of methane (CH_4), has four- to fivefold higher than that of hydrogen.³ Hence, great efforts have been made to increase the volumetric energy of hydrogen.⁴ On the other hand, we also concern how to reduce the atmospheric carbon dioxide (CO_2), which is the major greenhouse gas in Earth's atmosphere.^{5,6}

To solve these issues, H_2 storage through hydrogenation of CO_2 to hydrocarbons has been successfully developed.^{7,8} Ideally, this concept provides an alternative and sustainable pathway for H_2 storage by considering greenhouse gas CO_2 as a potential building block.⁹ It allows H_2 to be converted into renewable fuel, which directly resolves both global environment and H_2 storage issues. Among many alternative processes, photohydrogenation of CO_2 , which is an ideal method for converting CO_2 into desired fuels, is considered with much attention.¹⁰⁻¹² However, it is noted that the quantum efficiency and product yield in the CO_2 photohydrogenation are still low and requires a further study. The design of photocatalyst which works efficiently for the photohydrogenation of CO_2 has been the subject of several studies. Among the candidates, titania-supported copper catalyst plays a crucial role in promoting the photocatalytic reduction of CO_2 .¹³⁻¹⁶ Additionally, supported copper is found to be economical and abundant in nature.

Herein, a series of Cu/CuO loaded TiO₂ was synthesized and carried out the photohydrogenation of CO₂ with H₂O in the single photoreactor. It is noticeable that the oxidation state of Cu species is a crucial factor in CO₂ photoreduction activity.¹⁵ Hence, the impact of reducing CuO to Cu and the transition of Cu species during the reaction were carefully evaluated for their potential to hydrogenation. Furthermore, chemical and structural features of photocatalysts were thoroughly characterized by SEM, XRD, UV-vis, XPS and XANES.

2. Experimental

2.1. Preparation of photocatalysts

The whole synthesis procedure is shown in Scheme 1. Titanium dioxide (denoted as TiO₂) photocatalyst was prepared by a sol-gel method, which was adapted from Tseng et al.¹⁵ A typical batch contained 21 ml titanium (IV) butoxide (Ti(OC₄H₉)₄, 99 %, Fluka), 22 ml *n*-butanol (C₄H₉OH, 99.4 %, J.T. Baker) and 14 ml acetic acid (CH₃COOH, 99.7 %, J.T. Baker). The mixed solution was stirred for 8 h. Then, the transparent sol was dried at room temperature to 423 K for 3 h in an oven, then transferred to a furnace and calcined at 773 K for 5 h to burn off hydrocarbons and consequently produce the desired TiO₂ powder photocatalyst.

Titania-supported copper oxide (denoted as CuO/TiO₂) photocatalyst was prepared by an impregnation method. TiO₂ powder, which was previously prepared, was added to an appropriate amount of copper (II) chloride solution (CuCl₂, 99 %, Sigma-Aldrich). The solution was then sonicated in an ultrasonic bath and mixed with a magnetic stirrer to get a homogeneous slurry. After wet impregnation, it was dried at 353 K and finally calcined in air at 773 K for 4 h. For titania-supported copper metal (denoted as Cu/TiO₂) photocatalyst, it was prepared by reducing

of CuO/TiO₂ under a flow of 5% H₂/N₂ mixture at 573 K for 3 h. In our research, we named each photocatalyst with different Cu/CuO loading weight percentage.

2.2. Characterization of photocatalysts

The light absorption of photocatalysts was fully characterized by UV-visible spectrophotometer (UV-vis, Varian Cary-100). BaSO₄ was used as the absorption standard in these measurements. Powder X-ray diffractometer (XRD, Bruker-D8-ADVANCE) with a Cu K α ($\lambda = 1.5418\text{\AA}$) radiation source at 40 kV and 40 mA was used to verify the crystalline structure of the photocatalysts. The BET specific surface area of photocatalyst was determined by N₂ adsorption using Physisorption Analyzer (Micromeritics ASAP 2000). Field emission scanning electron microscopy (FE-SEM, JEOL JSM-7000) integrated with energy dispersive spectroscopy (EDS) was operated at an acceleration voltage of 5 kV. The photocatalysts were sputtered with a thin layer of Pt film to prevent surface charging. The X-ray photoelectron spectroscopy (XPS, Thermo Scientific Theta Probe) was used to determine the oxidation states of the elements. The X-ray absorption near-edge structure (XANES) at the Cu K-edge was recorded at the BL17C1 beamline, National Synchrotron Radiation Research Center (NSRRC), Taiwan, where the electron storage ring was operated at an acceleration voltage of 1.5 GeV. All data were acquired at an ambient temperature in the fluorescence mode. The K-edge data was normalized to equal the edge jump.

2.3. Photocatalytic hydrogenation of CO₂

The gas-phase photocatalytic hydrogenation of CO₂ with H₂O was carried out in a single Pyrex photoreactor with the volume of 385 ml (as shown in Figure 1). Photocatalyst powder (0.10 g) was evenly packed on the Teflon flat that was fixed in the middle of photoreactor. The bottom of photoreactor was moisturized with 5 ml of deionized water to tune the saturated water vapor pressure in the photoreactor through controlling the reaction temperature. The pen-ray lamp (11SC-1, 254 nm, 12 mW cm⁻²) was put from the top of photoreactor to irradiate the UV-light. Before the photoreactions, the reactor was first purged with the CO₂ for 30 min, and tightly closed at an ambient pressure. Then, H₂ (0.01 atm) was added to the photoreactor. After that, the photoreactor was heated up to 363 K by heating tape to generate the gaseous H₂O, and the lamp was switched on to start the experiment.

The reaction products collected in the gas phase were analyzed every 2 h during the irradiation by gas chromatography (China GC-FID 9800) integrated with the flame ionization detector. To analyze the CO, a methanizer packed with Ni catalyst was connected to GC-FID to convert CO into CH₄ with H₂ at 633 K. A Porapak Q column was installed, and pure N₂ was used as the carrier gas for FID in the detection of hydrocarbons.

The photoreduction quantum efficiency (PQE) is calculated as follows:

$$\text{PQE (\%)} = 100\% \times (n \times \text{product formation rate}) / \text{incident photon rate} \quad (1)$$

Here, n is the number of moles of photoelectrons required to generate one mole of reduction product from CO₂, which includes CH₄ and CO. The incident photon rate is determined from the incident light intensity at $\lambda = 254$ nm and projected light irradiation area.

The blank experiments were also conducted before performing the photocatalytic reaction. There were almost no products or below the detection limit of gas chromatography with any part

missing, including (a) photocatalysts and (b) UV-light source. Evidently, the photocatalytic hydrogenation of CO₂ is mainly photo-catalyzed.

3. Results and discussion

3.1. Photocatalyst characterization

All photocatalysts were fully characterized by BET, FE-SEM, EDS, UV-vis, XRD, XPS and XANES to reveal their structure, surface morphology and chemical state of the species. Firstly, the morphology of the synthesized TiO₂ and Cu-loaded TiO₂ is examined by FE-SEM, as shown in Figure 2. It clearly indicates that loading of Cu obviously could not change the shape and modify the morphology of supported TiO₂. However, the dispersion of Cu species might decrease with increasing loading amount. The mapping photograph for 2%CuO/TiO₂ photocatalyst and their corresponding elemental mapping of Ti, O and Cu was shown in Figure 3. It clearly shows that a part of the Cu-loaded could be aggregated. It is not beneficial for the photocatalytic activity. By the elemental EDS analysis, the weight percentages of Cu species in 1%Cu/TiO₂ and 2%Cu/TiO₂ are 0.95 and 2.31 wt%, respectively, which is consistent with the composition as planned.

Figure 4 depicts the XRD patterns of the TiO₂ along with Cu-loaded TiO₂ photocatalysts. All the photocatalysts exhibited similar XRD patterns. A very sharp and intense peak was observed at $2\theta = 25.28^\circ$ corresponds to the (101) planes of the anatase TiO₂, while few small peaks were also observed at 2θ values of 36.95° , 37.80° , 38.58° , 48.05° , 53.89° , 55.06° , 62.69° , 68.76° , 70.31° , 75.03° , and 76.02° , respectively. These values are in good agreement with anatase phase (JCPDS, No. 21-1272), suggesting that crystallite structure of TiO₂ exists mostly as anatase phase. The

inset of Figure 4 shows the shift of the (101) planes of the anatase TiO₂ peaks toward lower 2θ values in the patterns of Cu-loaded TiO₂, suggesting that Ti sites in the TiO₂ lattice were occupied by Cu species.¹⁷ Although we have observed the (101) planes of the anatase TiO₂ peaks changed significantly in intensity, only a slight change in half width was observed. The TiO₂ crystallite sizes were estimated from the half bandwidth of the corresponding X-ray spectral peak by the Scherrer formula:

$$D = k\lambda/(\beta \cos\theta) \quad (2)$$

Here, λ is the X-ray wavelength ($\lambda = 1.5418\text{\AA}$), β is the half width of the (101) planes, θ is the Bragg diffraction angle, and k is a correction factor ($k = 0.9$).

In this study, the TiO₂ crystallite sizes were about 31.4-34.0 nm (Table 1), which is consistent with SEM result. It is noted that there are no apparent peaks for CuO in the XRD patterns of CuO/TiO₂. The reason is that the amount of Cu species is very low, in the range of 1-2 wt%; hence, it could not be ruled out due to limitations of the experimental technique. For Cu/TiO₂, the peak at 2θ values of 43.3° and 50.4°, corresponding to Miller indices (111) and (200) planes of metallic Cu species, respectively.¹⁸

The optical properties of the TiO₂ together with Cu-loaded TiO₂ photocatalysts are measured by UV-vis spectra. As displayed in Figure 5, it clearly shows that all the photocatalysts performed the absorption peak of 360 nm, assigned to TiO₂. The Cu-loaded TiO₂ photocatalysts have an extended absorption edge in the region of 400-800 nm. Interestingly, the UV-Vis spectroscopic studies could gain information on the state of Cu species in these catalysts.¹⁹ As expected, the upward shift of intensity absorbance in this region increased with the loading amount of Cu species. It is noticeable that the broadband of CuO/TiO₂ photocatalysts in the range of 600-800

156 nm corresponds to d–d transitions of Cu^{2+} in Oh symmetry with a tetragonal distortion.¹⁷ This
157 observation implies that Cu^{2+} species was mainly presented on CuO/TiO_2 photocatalysts.
158 Additionally, pretreatment the photocatalyst by H_2 to reduce the CuO to Cu will raise the band
159 located at 410–590 nm, which corresponds to metallic Cu^0 species.^{19, 20} It is noted that this range
160 is also associated with the three-dimensional Cu^{1+} clusters in the CuO matrix due to incomplete
161 reduction.¹⁹

162 The oxidation state of Cu species is a key factor that determines their photocatalytic activity in
163 the photoreduction of CO_2 .¹⁵ X-ray photoelectron spectroscopy (XPS) was conducted to
164 determine further the chemical environment of Cu species. XPS spectra of the $\text{Cu}2\text{p}$ region for
165 TiO_2 , 2% Cu/TiO_2 , and 2% CuO/TiO_2 photocatalysts are reported (Figure 6(a)). There is no peak
166 observed in the range of 925–965 eV for TiO_2 photocatalyst. In contrast, the $\text{Cu}2\text{p}_{3/2}$ and $\text{Cu}2\text{p}_{1/2}$
167 binding energy values of 2% CuO/TiO_2 photocatalyst appeared at 933.9 eV and 953.6 eV,
168 respectively, confirming the presence of Cu^{2+} . It is noted that pretreatment the 2% CuO/TiO_2
169 photocatalyst by H_2 to successfully reduce the Cu^{2+} to Cu^0 . The $\text{Cu}2\text{p}_{3/2}$ and $\text{Cu}2\text{p}_{1/2}$ binding
170 energy values of 2% Cu/TiO_2 photocatalyst appeared at 931.6 eV and 951.8 eV, respectively.
171 These results are in accordance with an earlier report.²¹ Due to the low amount of Cu species on
172 1% CuO/TiO_2 and 1% Cu/TiO_2 samples, its XPS spectra of the $\text{Cu}2\text{p}$ region could not be
173 observed clearly. Figure 6(b) shows the $\text{Ti}2\text{p}$ region for TiO_2 , 2% Cu/TiO_2 , and 2% CuO/TiO_2
174 photocatalysts. The binding energy values appeared at 458.7 eV and 457.3 eV corresponded to
175 Ti^{4+} and Ti^{3+} , respectively.²² There is a significant amount of Ti^{3+} rather than Ti^{4+} observed in the
176 $\text{Ti}2\text{p}$ XPS spectra of 2% Cu/TiO_2 , and 2% CuO/TiO_2 , in compared with TiO_2 photocatalysts. On
177 the other hand, we also observed a shift to higher binding energy for O1s spectra when Cu
178 species was introduced to the TiO_2 (Figure 6(c)). The O1s binding energy of TiO_2 was at 529.9

179 eV while those of Cu-loaded/TiO₂ was at 530.6 eV. The loading Cu could modify the surface
180 hydroxyl (O_H) content of photocatalyst.²³

181 To have a clearer image of the Cu state on 1%Cu/TiO₂ and 1%CuO/TiO₂ photocatalysts, Cu K-
182 edge XANES was characterized. Figure 7(a) shows the Cu K-edge XANES spectra of
183 1%Cu/TiO₂ and 1%CuO/TiO₂ photocatalysts, in compared with the Cu foil, Cu₂O and CuO
184 references. The good resemblance spectra of 1%Cu/TiO₂ and 1%CuO/TiO₂ with that of Cu foil
185 and CuO references indicates that their local structure in 1%Cu/TiO₂ and 1%CuO/TiO₂
186 photocatalysts are mainly in Cu⁰ and Cu²⁺, respectively. There are four types of peaks in a range
187 of 8960-9040 eV, including 1s-3d transition (A), 1s-4p_z (1s-4pπ*) transition (B), 1s-4p_{x,y} (1s-
188 4pσ*) transition (C), and multiple scattering (D).²⁴ The spectrum of 1%CuO/TiO₂ exhibits a
189 well-separated weak pre-edge band A due to the 1s-3d transition and an intense band B and C
190 due to the 1s-4p transition. However, the band B, which could be observed as a shoulder of the
191 intense band C, is not clearly separated. Additionally, with the presence of a band D (multiple
192 scattering), it suggests that the Cu species on 1%CuO/TiO₂ are aggregated.²⁴ For the 1%Cu/TiO₂
193 spectrum, there are no peaks attributed to the band A and D. More importantly here, the Fourier
194 transforms (FTs) of the $k^3\chi(k)$ EXAFS for 1%Cu/TiO₂ and 1%CuO/TiO₂ photocatalysts along
195 with Cu foil, Cu₂O, and CuO references were also compared in Figure 7(b). Phase shift function
196 was used as reference files to analyze the EXAFS data. In the 1%Cu/TiO₂ photocatalyst, the FT
197 peak appearing at 2.45 Å is assigned to Cu-Cu bond. In the 1%CuO/TiO₂ photocatalyst, the first
198 FT peak appearing at 1.84 Å is assigned to Cu-O bond. However, different from the above
199 XANES result, the FT for 1%CuO/TiO₂ photocatalyst in the range of 2-4 Å is not similar to that
200 for the CuO reference but is somewhat similar to that for the Cu₂O reference. In particular, it
201 exhibits only one peak appearing at 3.00 Å, which is assigned to Cu-Cu bond.

In summary, Cu species were successfully loaded on TiO₂ using the incipient wetness impregnation method. Based on the UV-vis, XRD, XPS, and XANES results, the Cu²⁺ mainly exists on CuO/TiO₂ photocatalyst. Importantly, most Cu species in the photocatalysts was stable in Cu⁰ after reduction by H₂. The presence of Cu species exhibits outstanding the optical properties. It expects that Cu-loaded TiO₂ can significantly influence the photoreduction of CO₂.

3. Photocatalytic hydrogenation of CO₂

3.1 The presence of hydrogen and reaction temperature

Figure 8 shows the time profiles of the photocatalytic reduction of CO₂ with H₂O in the presence/absence of H₂ under different temperature on 1%Cu/TiO₂ photocatalyst. Firstly, we conducted the photoreduction of CO₂ with H₂O at 333 K without H₂. The result shows that only 0.07 μmol g⁻¹ of CH₄ and no CO product were formed after 8 h in condition.

By increasing the reaction temperature to 363 K, both CH₄ and CO are detected. Their product yields are 5.32 and 0.26 μmol g⁻¹ for CH₄ and CO, respectively, after 8 h of reaction. It is accepted that photon irradiation is the primary source of energy in photocatalysis to generate the electron-hole pairs at an ambient temperature. However, the photocatalytic reactions proceed more efficiently at high temperatures because the surface reaction can be accelerated by raising the collision frequency and diffusion rate.²⁵ Furthermore, products do not easily be desorbed at low temperatures; on the contrary, it desorbs more readily at high temperatures. It should be mentioned that H₂O vapor plays a crucial role in the photocatalytic activity. Further raising the reaction temperature also increases the generated gaseous H₂O, resulting in the enhancement of photocatalytic activity. Several studies have focused on the reaction temperature dependence of

the photocatalytic activity.²⁵⁻²⁷ Note that Anpo et al. also carried out the photoreduction of CO₂ with H₂O on various TiO₂ catalysts.²⁶ They reported that their enhancement of product yields corresponds to the reaction temperature and amount of gaseous H₂O, which is highly consistent with this study.

Investigation of photohydrogenation of CO₂ at 363 K in the presence of H₂ was also conducted. The result shows that it took 2 h for CO to reach a maximum yield (5.47 μmol g⁻¹), and then it gradually decreased. In general, CO is thermodynamically more favorable than CO₂.¹¹ Hence, it might be consumed by reacting with either H₂ or H₂O to produce CH₄, resulting in the observed decrease of CO yield. For the yield of CH₄, it is in a good linear relationship with the irradiation time. The CH₄ yield reaches to 28.72 μmol g⁻¹ after 8 h in reaction. Such significant improvement of photocatalytic reaction is attributed to the presence of H₂, which is used immediately for the hydrogenation of CO₂. The reason is that hydrogenation of CO₂ is thermodynamically favorable and is a spontaneous reaction.

237

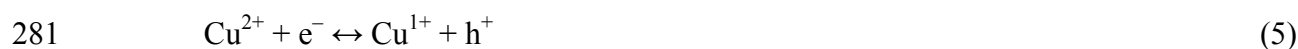
3.2 The amount Cu-loaded and its oxidation state on TiO₂ supports

The influence of amount CuO-loaded TiO₂ on photohydrogenation of CO₂ with H₂O was also examined at 363 K. As expected, Figure 9 shows that the catalysts with a CuO loading of 1 and 2 wt.% exhibited photocatalytic reactivity to produce CO and CH₄ with a yield of 4.0-5.0 and 19.3-14.6 μmol g⁻¹, respectively. Note that only 1.33 μmol g⁻¹ of CO and 11.94 μmol g⁻¹ of CH₄ were produced over TiO₂ under the same condition. It is well known that the recombination of the electron-hole pair will be reduced when Cu species is loaded on TiO₂. Hence, the photoactivity will be enhanced with the loading of Cu species. Additionally, Ti³⁺ species are an important

factor that influences the photocatalytic activity in the photohydrogenation of CO₂. The reason is that the electron-rich Ti³⁺ species might transfer spontaneously an electron to surface adsorbed CO₂ leading to an intermediate CO₂^{•−} species.²⁸ As it can be noticed, CO₂^{•−} species is supported as the precursor of CO formation. It is important to emphasize that following the loading Cu species on TiO₂ support, the ratio of Ti³⁺ species, which is shown in Figure 6(b), will increase dramatically compared with TiO₂. Hence, the observed yield of CO was increased more than threefold by Cu-loaded species. On the other hand, the surface hydroxyl content of photocatalyst was observed to increase with the presence of Cu-loaded (Figure 6(c)). It is noted that the surface hydroxyl is the crucial role to enhance the photocatalytic activity by generating the active hydroxyl radicals.²⁹

Although the adding CuO species improves significantly the activity, the addition of excess CuO to TiO₂ was undesirable for the photoreaction. Firstly, one of the influential factors of this dependence may be the CuO dispersion on TiO₂. The CuO dispersion usually decreases with increasing loading amount because of the aggregation of some small CuO particles, resulting in the reduced surface illumination of the photocatalyst. Note that BET surface area of 1%CuO/TiO₂ and 2%CuO/TiO₂ photocatalysts are 6.1 and 3.8 m² g^{−1}, respectively (Table 1). A loss of 38% of BET surface area was observed by increasing the loading CuO amount from 1% to 2%. The previous study observed that CuCl₂ precursor, which was also used in this study, led to being well-dispersed Cu at low loading only.^{30, 31} At high loading, a significant amount of CuO species aggregated on the surface of the support and obscured the pores of TiO₂. Secondly, excess CuO might act as the recombination centers for electron-hole pairs, resulting in reduced photoactivity.

The oxidation state of Cu species is also a key factor that determines their CO₂ photoreduction activity.¹⁵ In this study, the pretreatment 1%CuO/TiO₂ by reducing CuO to Cu was found to be more efficient to generate CH₄ than that without pretreatment (Figure 10). The yield of CH₄ for Cu/TiO₂ was 28.72 μmol g⁻¹, which was enhanced 48.5% compared with that for CuO/TiO₂. To gain further insight into the transition of the nature of the copper species during the reaction, the photocatalysts was collected after the experiment for further XPS and UV-vis analysis. Figure 11 shows that the Cu2p peaks for spent CuO/TiO₂ photocatalyst, which was collected after the reaction, were shifted to lower binding energy than those for fresh CuO/TiO₂ photocatalyst. On the other hand, the Cu2p peaks for spent Cu/TiO₂ photocatalyst were shifted to higher binding energy than those for fresh Cu/TiO₂ photocatalyst. This result reveals that Cu¹⁺ species could be generated during UV-light irradiation from a part of either Cu⁰ or Cu²⁺ species.



During the photoreaction, the holes and electrons from TiO₂ can be transferred to Cu⁰ and Cu²⁺ species to keep a certain amount of their species oxidized and reduced, respectively, to Cu¹⁺.³² The UV-vis analysis of above photocatalysts is also shown in Figure 11. In details, the UV-vis spectrum of the spent Cu/TiO₂ photocatalyst shows an increased intensity in the range of 410-590 nm, in compared with that of the fresh Cu/TiO₂ photocatalyst. This change indicates that a part of Cu⁰ was oxidized to Cu¹⁺ species.¹⁹ Similarly, we also observed this phenomenon for spent CuO/TiO₂ photocatalyst, confirming the presence of Cu¹⁺ species. The UV-vis result agrees with the XPS result. We final note that CuO-Cu₂O/TiO₂ and Cu-Cu₂O/TiO₂

photocatalysts system could be formed under UV-light irradiation (Figure 11). Briefly, the co-existence of different nature of Cu species has a significant influence on the photocatalytic activity by the enhanced separation and inhibited recombination of photogenerated electron-hole pairs. Moreover, it also exhibits outstanding the optical properties. Especially, the Cu-Cu₂O/TiO₂ structure is proposed can also further prolong the lifetime of electrons. The reason is that the electrons, which is generated by UV-light irradiation on the Cu₂O valence band, need to transfer to the media Cu first, and then further transfer to the valence band of TiO₂.³² As a result, Cu-Cu₂O/TiO₂ had the highest photocatalytic performance, among candidate photocatalysts. Interestingly, Cu-Cu₂O/TiO₂ also performed an excellent selectivity to CH₄ yield. The reasons are that Cu⁰ species could efficiently suppress the formation of CO,³³ while Cu¹⁺ species is noted as an active site to promote the formation of CH₄ efficiently.³⁴

3.3 Comparison of the photoreduction efficiency

The dependencies of products yield and PQE on different photocatalysts are shown in Figure 12. The results suggest that Cu-loaded TiO₂ reduces CO₂ more efficiently than TiO₂. The photohydrogenation activity is intensively related to the amount Cu-loaded and its oxidation state on TiO₂. The increased photocatalytic activity with the presence of Cu species can be explained as Cu species acting as electron traps responsible for accumulating the photo-generated electrons, and resulting in minimizing charge recombination electron-hole pairs. Additionally, the ratio of Ti³⁺ species in Cu-loaded TiO₂ was higher than that in TiO₂. This observation is attributed to the enhancement of CO formation. However, adding excess CuO/Cu to TiO₂ may face the low dispersion issue resulting in the activity inhibition. In the present, we observed that PQE achieved highest over 1%Cu/TiO₂ photocatalyst (0.13%).

Although the conditions for conducting experiments are different, it is worth comparing the photocatalytic activity regarding product rate in the literature (Table 2).^{17, 35-41} We see that CO and CH₄ were formed as the main products. Despite substantial efforts have been devoted to improving the efficiency of this photocatalytic process, it is still lower than in natural photosynthesis. Hence, further research in this field is needed for enabling photohydrogenation / photoreduction of CO₂ in the future.

4. Conclusions

Cu species (Cu⁰ and Cu²⁺) were successfully loaded on the TiO₂ support and then evaluated for their potential to hydrogenation of CO₂. There might exist the interaction between the Cu species and TiO₂ support that enhancing a significant amount of Ti³⁺ rather than Ti⁴⁺ species in Cu-loaded TiO₂, in compared with TiO₂ photocatalysts. This property provides a chance to generate an intermediate CO₂^{•-} species, leading to the enhancement of CO₂ hydrogenation activity. Notably, CuO-Cu₂O/TiO₂ and Cu-Cu₂O/TiO₂ photocatalyst system, which was formed under UV-light irradiation, significantly enhanced photocatalytic activity by prolonging the lifetime of electrons. The co-existence of Cu⁰ and Cu¹⁺ species was beneficial to catalysis involving hydrogenation of CO₂ into desired renewable fuel (CH₄). Although the adding Cu species improves the activity significantly, the excess content of Cu to TiO₂ was undesirable for the photoreaction. To achieve the enhanced photocatalytic activity, the content of Cu species must be maintained at an appropriate low concentration (≤ 1 wt.%), and the corresponding highest CH₄ yield was 28.72 μmol g⁻¹.

Acknowledgments

The authors kindly thank the Ministry of Science and Technology, Taiwan for financially supporting this research under the project MOST 103-2923-E-002-009-MY3 and the Grant Agency of the Czech Republic (14-35327J).

References

1. D. Lozano-Castelló, F. Suárez-García, Á. Linares-Solano and D. Cazorla-Amorós, in *Renewable Hydrogen Technologies*, ed. L. M. G. A. M. Diéguez, Elsevier, Amsterdam, 2013, DOI: <http://dx.doi.org/10.1016/B978-0-444-56352-1.00012-X>, pp. 269-291.
2. S. Kumar, in *Clean Hydrogen Production Methods*, Springer International Publishing, 2015, DOI: 10.1007/978-3-319-14087-2_1, ch. 1, pp. 1-9.
3. F. Amrouche, A. Benzaoui, P. Erickson, B. Mahmah, F. Herouadi and M. Belhamel, *Int. J. Hydrogen Energy*, 2011, **36**, 4094-4102.
4. A. Züttel, *Naturwissenschaften*, 2004, **91**, 157-172.
5. N. P. Gillett, V. K. Arora, D. Matthews and M. R. Allen, *J. Climate*, 2013, **26**, 6844-6858.
6. S. Protti, A. Albini and N. Serpone, *Phys. Chem. Chem. Phys.*, 2014, **16**, 19790-19827.
7. A. Züttel, P. Mauron, S. Kato, E. Callini, M. Holzer and J. Huang, *CHIMIA Int. J. Chem.*, 2015, **69**, 264-268.
8. S. Saeidi, N. A. S. Amin and M. R. Rahimpour, *J. CO2 Utilization*, 2014, **5**, 66-81.
9. T. Müller, W. Leitner, P. Markewitz and W. Kuckshinrichs, in *Carbon Capture, Storage and Use*, eds. W. Kuckshinrichs and J.-F. Hake, Springer International Publishing, 2015, DOI: 10.1007/978-3-319-11943-4_4, ch. 4, pp. 67-100.
10. X. Yang, S. Kattel, S. D. Senanayake, J. A. Boscoboinik, X. Nie, J. Graciani, J. A. Rodriguez, P. Liu, D. J. Stacchiola and J. G. Chen, *J. Am. Chem. Soc.*, 2015, **137**, 10104-10107.
11. Y.-H. Cheng, V.-H. Nguyen, H.-Y. Chan, J. C. S. Wu and W.-H. Wang, *Appl. Energy*, 2015, **147**, 318-324.

- 362 12. S.-H. Yu, C.-W. Chiu, Y.-T. Wu, C.-H. Liao, V.-H. Nguyen and J. C. S. Wu, *Appl. Catal.*
363 *A: Gen.*, DOI: <http://dx.doi.org/10.1016/j.apcata.2015.08.027>.
- 364 13. K. Hirano, K. Inoue and T. Yatsu, *J. Photochem. Photobiol., A: Chem.*, 1992, **64**, 255-
365 258.
- 366 14. J. C. S. Wu, H.-M. Lin and C.-L. Lai, *Appl. Catal. A: Gen.*, 2005, **296**, 194-200.
- 367 15. I. H. Tseng, J. C. S. Wu and H.-Y. Chou, *J. Catal.*, 2004, **221**, 432-440.
- 368 16. I. H. Tseng, W.-C. Chang and J. C. S. Wu, *Appl. Catal. B: Environ.*, 2002, **37**, 37-48.
- 369 17. F. Gonell, A. V. Puga, B. Julián-López, H. García and A. Corma, *Appl. Catal. B:*
370 *Environ.*, 2016, **180**, 263-270.
- 371 18. S.-H. Wu and D.-H. Chen, *J. Colloid Interface Sci.*, 2004, **273**, 165-169.
- 372 19. H. Praliaud, S. Mikhailenko, Z. Chajar and M. Primet, *Appl. Catal. B: Environ.*, 1998, **16**,
373 359-374.
- 374 20. L. Chen, T. Horiuchi, T. Osaki and T. Mori, *Appl. Catal. B: Environ.*, 1999, **23**, 259-269.
- 375 21. B. Srinivas, B. Shubhamangala, K. Lalitha, P. Anil Kumar Reddy, V. Durga Kumari, M.
376 Subrahmanyam and B. R. De, *Photochem. Photobiol.*, 2011, **87**, 995-1001.
- 377 22. V.-H. Nguyen, H.-Y. Chan and J. C. S. Wu, *J. Chem. Sci.*, 2013, **125**, 859-867.
- 378 23. M. You, T. G. Kim and Y.-M. Sung, *Cryst. Growth Des.*, 2010, **10**, 983-987.
- 379 24. H. Yamashita, M. Matsuoka, K. Tsuji, Y. Shioya, M. Anpo and M. Che, *J. Phys. Chem.*,
380 1996, **100**, 397-402.
- 381 25. V.-H. Nguyen, J. C. S. Wu and H. Bai, *Catal. Comm.*, 2013, **33**, 57-60.
- 382 26. M. Anpo, H. Yamashita, Y. Ichihashi and S. Ehara, *J. Electroanal. Chem.*, 1995, **396**, 21-
383 26.
- 384 27. X. Fu, L. A. Clark, W. A. Zeltner and M. A. Anderson, *J. Photochem. Photobiol., A:*
385 *Chem.*, 1996, **97**, 181-186.
- 386 28. Ş. Neaţu, J. A. Maciá-Agulló, P. Concepción and H. Garcia, *J. Am. Chem. Soc.*, 2014,
387 **136**, 15969-15976.
- 388 29. W. Lu, S. Gao and J. Wang, *J. Phys. Chem. C*, 2008, **112**, 16792-16800.
- 389 30. X. Bokhimí, A. Morales, O. Novaro, T. López, O. Chimal, M. Asomoza and R. Gómez,
390 *Chem. Mater.*, 1997, **9**, 2616-2620.
- 391 31. O. Ola and M. Mercedes Maroto-Valer, *Catal. Sci. Technol.*, 2014, **4**, 1631-1637.

- 392 32. Z. Xi, C. Li, L. Zhang, M. Xing and J. Zhang, *Int. J. Hydrogen Energy*, 2014, **39**, 6345-
393 6353.
- 394 33. G. Wu, T. Chen, G. Zhou, X. Zong and C. Li, *Sci. China, Ser. B: Chem.*, 2008, **51**, 97-
395 100.
- 396 34. S. Zhu, S. Liang, Y. Tong, X. An, J. Long, X. Fu and X. Wang, *Phys. Chem. Chem. Phys.*,
397 2015, **17**, 9761-9770.
- 398 35. D. Liu, Y. Fernández, O. Ola, S. Mackintosh, M. Maroto-Valer, C. M. A. Parlett, A. F.
399 Lee and J. C. S. Wu, *Catal. Comm.*, 2012, **25**, 78-82.
- 400 36. F. Bi, M. F. Ehsan, W. Liu and T. He, *Chin. J. Chem.*, 2015, **33**, 112-118.
- 401 37. K. Teramura, S.-i. Okuoka, H. Tsuneoka, T. Shishido and T. Tanaka, *Appl. Catal. B:*
402 *Environ.*, 2010, **96**, 565-568.
- 403 38. Q. Liu, Y. Zhou, Z. Tian, X. Chen, J. Gao and Z. Zou, *J. Mater. Chem.*, 2012, **22**, 2033-
404 2038.
- 405 39. C. Zhang, Q. Zhang, S. Kang, B. Li, X. Li and Y. Wang, *ECS Solid State Lett.*, 2013, **2**,
406 M49-M52.
- 407 40. S. K. Parayil, A. Razzaq, S.-M. Park, H. R. Kim, C. A. Grimes and S.-I. In, *Appl. Catal.*
408 *A: Gen.*, 2015, **498**, 205-213.
- 409 41. T. Wang, X. Meng, G. Liu, K. Chang, P. Li, Q. Kang, L. Liu, M. Li, S. Ouyang and J. Ye,
410 *J. Mater. Chem. A*, 2015, **3**, 9491-9501.
- 411

412 **Tables and Figures**

413 **Table 1.** The properties of TiO₂ supports

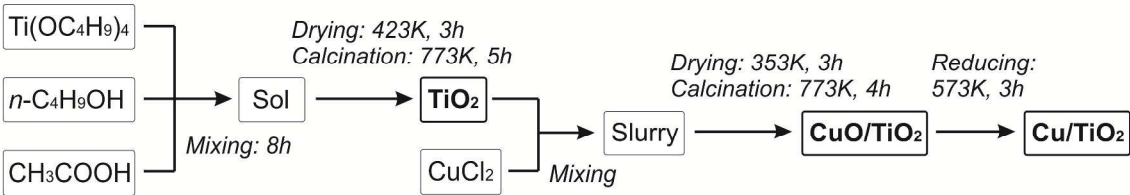
Entry	Photocatalysts	BET (m ² g ⁻¹)	TiO ₂ crystalline size (nm)
1	TiO ₂	5.2	31.4
2	1%CuO/TiO ₂	6.1	32.6
3	2%CuO/TiO ₂	3.8	32.6
4	1%Cu/TiO ₂	6.3	34.0
5	2%Cu/TiO ₂	5.1	33.9

414

415 **Table 2.** The performance comparison of photocatalytic activity

En try	Catalysts	Conditions			Products ($\mu\text{mol g}^{-1} \text{h}^{-1}$)	PQE (%)	Ref. / Year
		Reaction medium	Light source	Temp (K)			
1	Cu/TiO ₂	H ₂ O (5 mL), H ₂ (0.01 atm), saturated CO ₂ (1 atm)	11SC-1 pen-ray lamp: 254 nm; 12 mW cm ⁻²	363	CO: 0.54 CH ₄ : 3.59	0.13	This study
2		H ₂ O (5 mL), saturated CO ₂ (1 atm)			CO: 0.03 CH ₄ : 0.67	0.03	
3	Cu/TiO ₂	H ₂ O (200 mL), saturated CO ₂ (1 atm)	8 W UVA: 3.25 mW cm ⁻²	–	CH ₄ : 0.03	–	³⁵ / 2012
4	Cu ₂ O/TiO ₂	H ₂ O (100 mL), saturated CO ₂ (1.25 atm)	300 W xenon lamp (PLS-SXE300, $\lambda \geq 420$ nm)	288	CH ₄ : 0.16		³⁶ / 2015
5	3.0Cu-TiO ₂	H ₂ O (25 mL) under a CO ₂ atmosphere (1.4 bars)	Hg lamp (125 W)	298	CO: 0.3 CH ₄ : 0.3 H ₂ : 0.3	–	¹⁷ / 2016
6	LiTaO ₃	CO ₂ (150 μmol), H ₂ (50 μmol)	200 W Hg-Xe lamp (UVF-204S Type C)	303	CO: 0.42	–	³⁷ / 2010
7	RuO ₂ –Pt/ Zn _{1.7} GeN _{1.8} O	H ₂ O (0.4 ml), saturated CO ₂ (1 atm)	300 W Xe arc lamp ($\lambda > 420$ nm)	–	CH ₄ : 4.58	0.03	³⁸ / 2012
8	TiO ₂ -GCM	H ₂ O (5 ml), saturated CO ₂ (1 atm)	300 W Xe arc lamp	303	CH ₄ : 2.06	–	³⁹ / 2013
9	C ₃ N-TNT06	CO ₂ and H ₂ O vapors (80% humidity)	100 W Xenon with an AM 1.5 filter	–	CH ₄ : 9.75	–	⁴⁰ / 2015
10	Co-doped TiO ₂	H ₂ O (3 ml), a pure CO ₂ gas (80 kPa)	300 W xenon arc lamp with an L-42 glass filter	–	CO: 0.34 CH ₄ : 0.18	–	⁴¹ / 2015

Abbreviation: PQE: Photoreduction quantum efficiency, –: lack of information.



Scheme 1. The flow chart for synthesis procedure of photocatalysts.



Figure 1. The diagram of a single Pyrex photoreactor system.

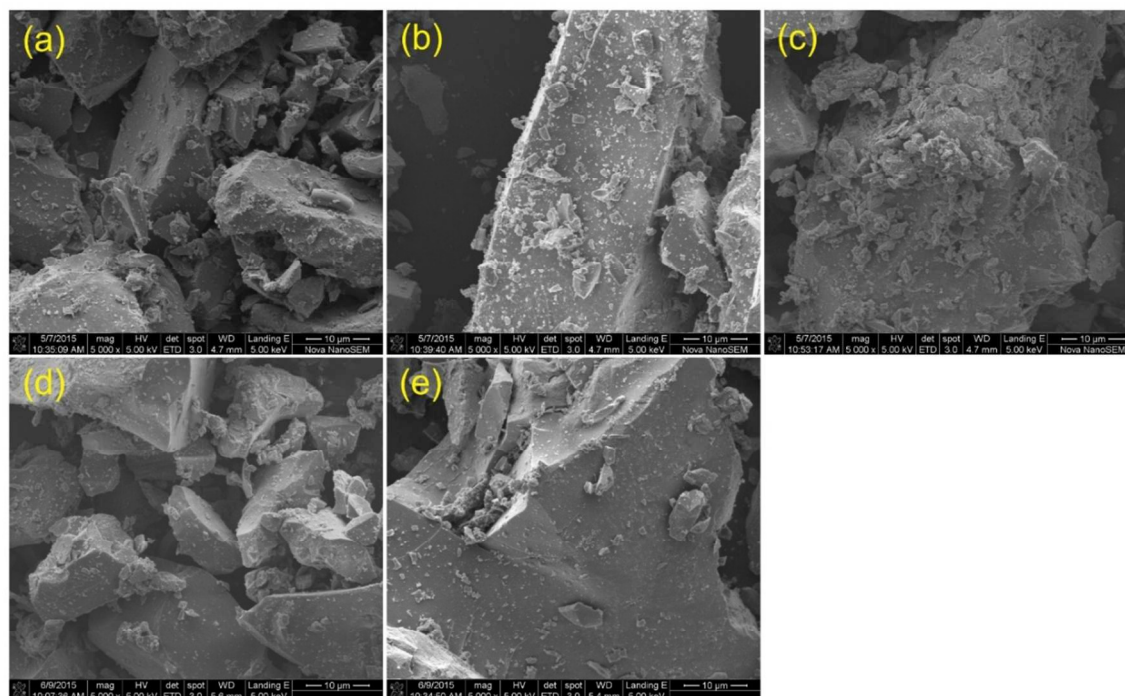


Figure 2. SEM images of (a) TiO_2 , (b) $1\%\text{CuO}/\text{TiO}_2$, (c) $2\%\text{CuO}/\text{TiO}_2$, (d) $1\%\text{Cu}/\text{TiO}_2$, and (e) $2\%\text{Cu}/\text{TiO}_2$ photocatalysts.

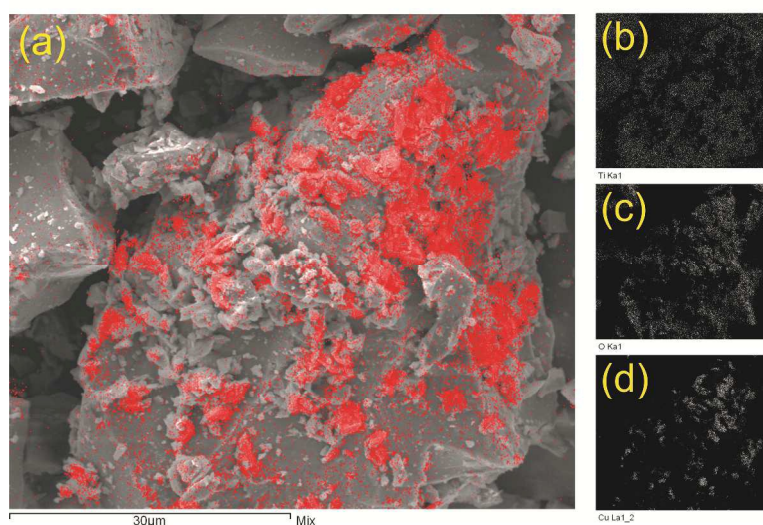


Figure 3. SEM mapping photograph for $2\%\text{CuO}/\text{TiO}_2$ photocatalyst: (a) SEM image of $2\%\text{CuO}/\text{TiO}_2$ with Cu mapping, and elemental mapping images of (b) Ti, (c) O, and (d) Cu.

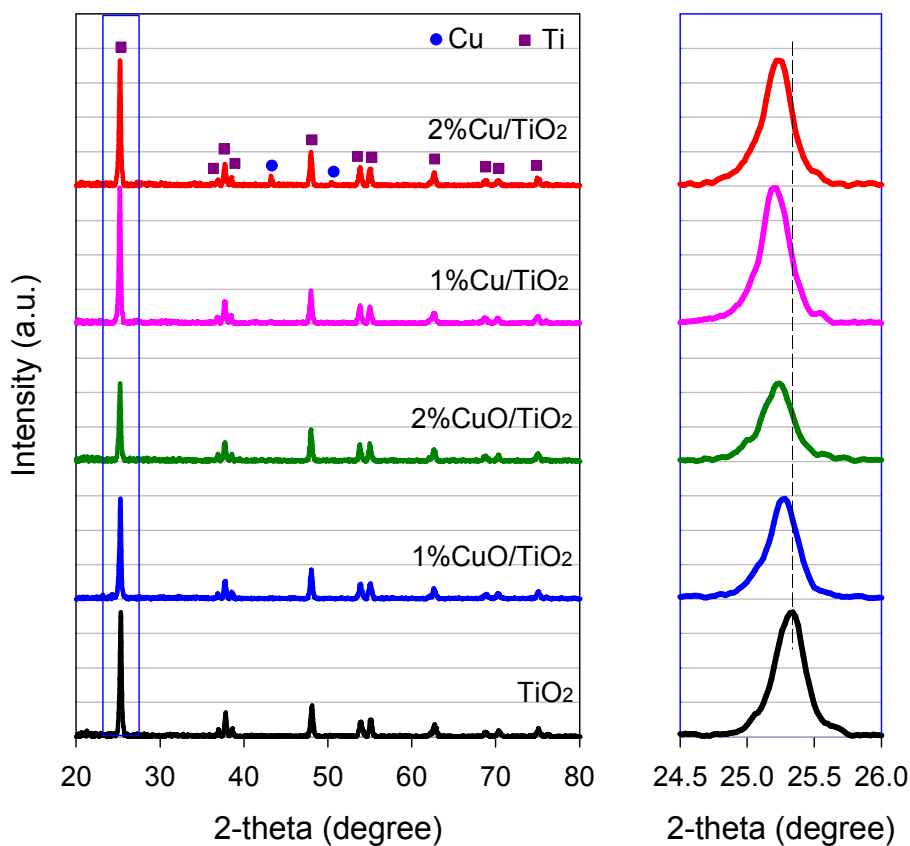


Figure 4. XRD patterns of TiO₂, 1%CuO/TiO₂, (c) 2%CuO/TiO₂, 1%Cu/TiO₂, and 2%Cu/TiO₂ photocatalysts. The inset depicts the shift of the (101) planes of TiO₂ supports.

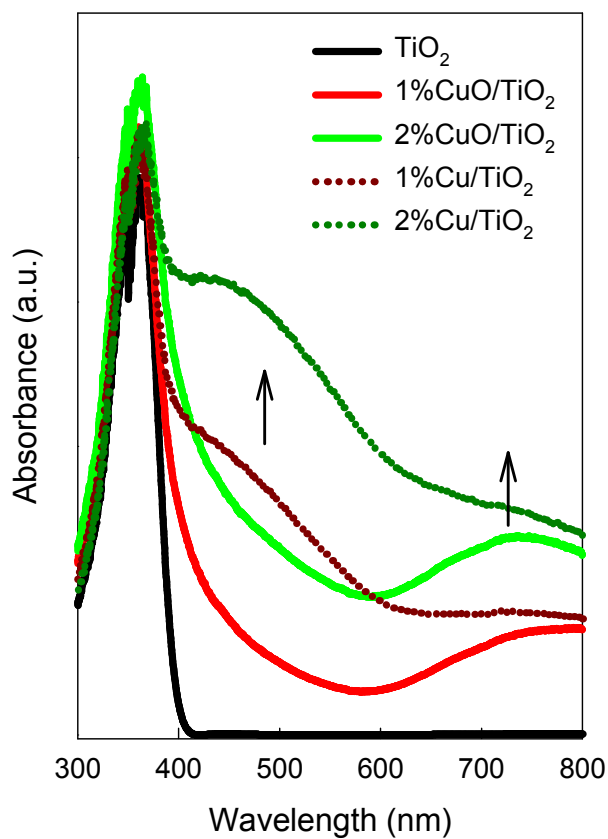


Figure 5. UV-vis spectra of TiO_2 , 1% CuO/TiO_2 , (c) 2% CuO/TiO_2 , 1% Cu/TiO_2 , and 2% Cu/TiO_2 photocatalysts.

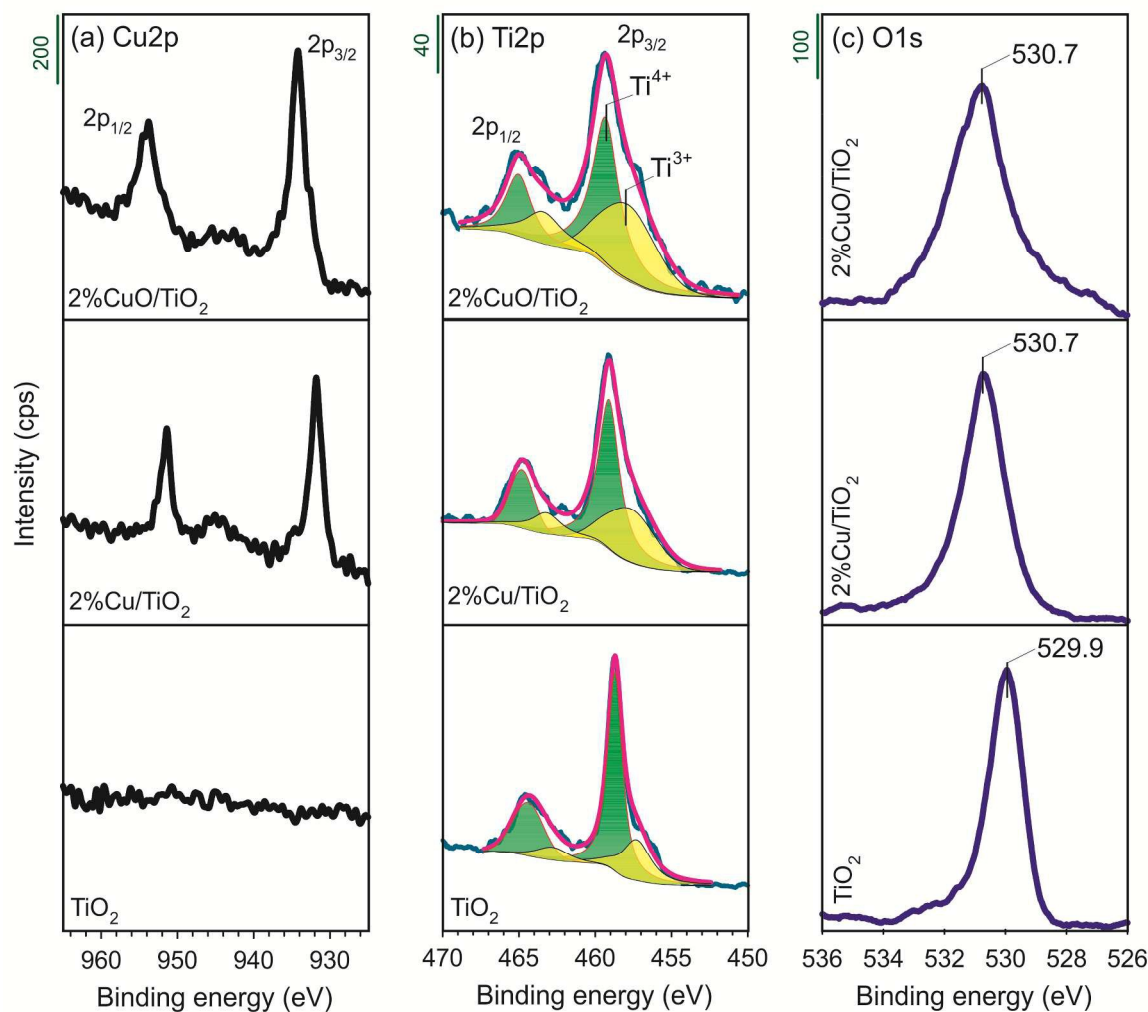


Figure 6. XPS spectra of (a) Cu2p, (b) Ti2p and (c) O1s for TiO₂, 2%Cu/TiO₂, and 2%CuO/TiO₂ photocatalysts.

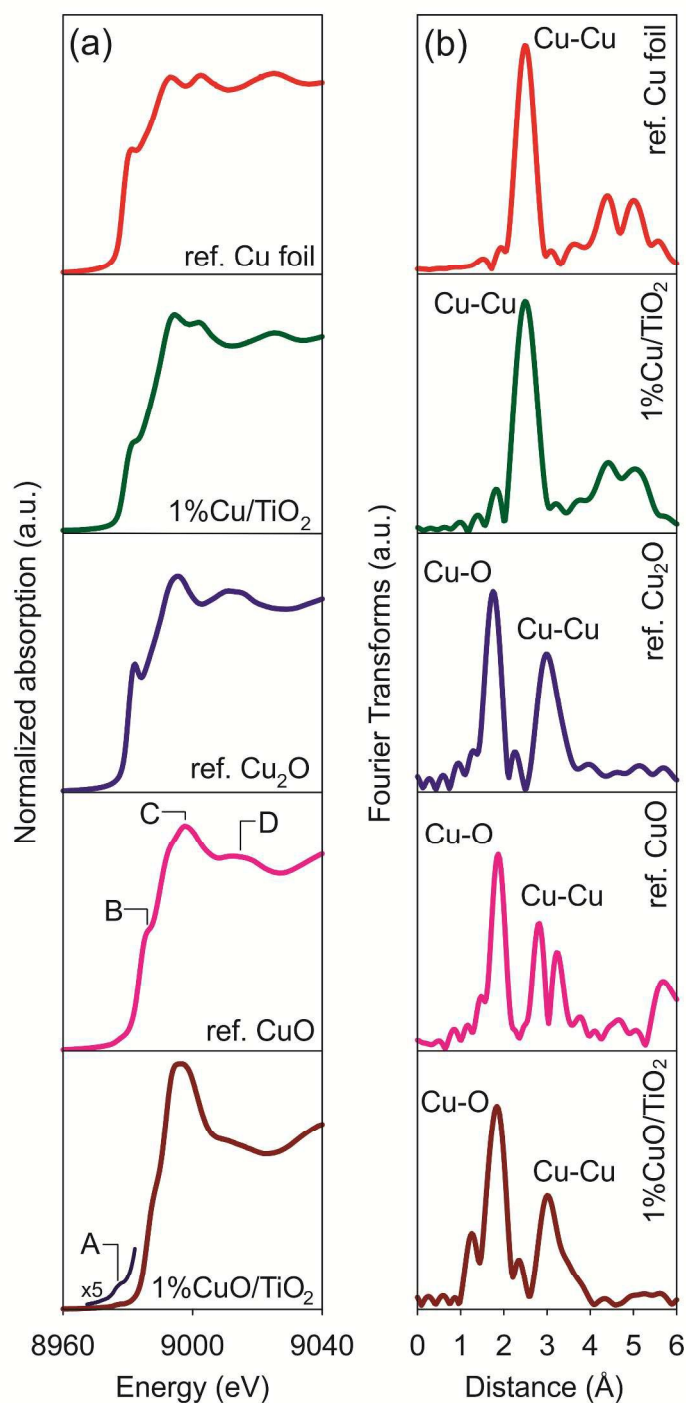


Figure 7. (a) Normalized Cu K-edge XANES spectra and (b) Fourier transforms of Cu K-edge EXAFS spectra for 1%Cu/TiO₂ and 1%CuO/TiO₂ photocatalysts, together with Cu metal foil, Cu₂O, and CuO references.

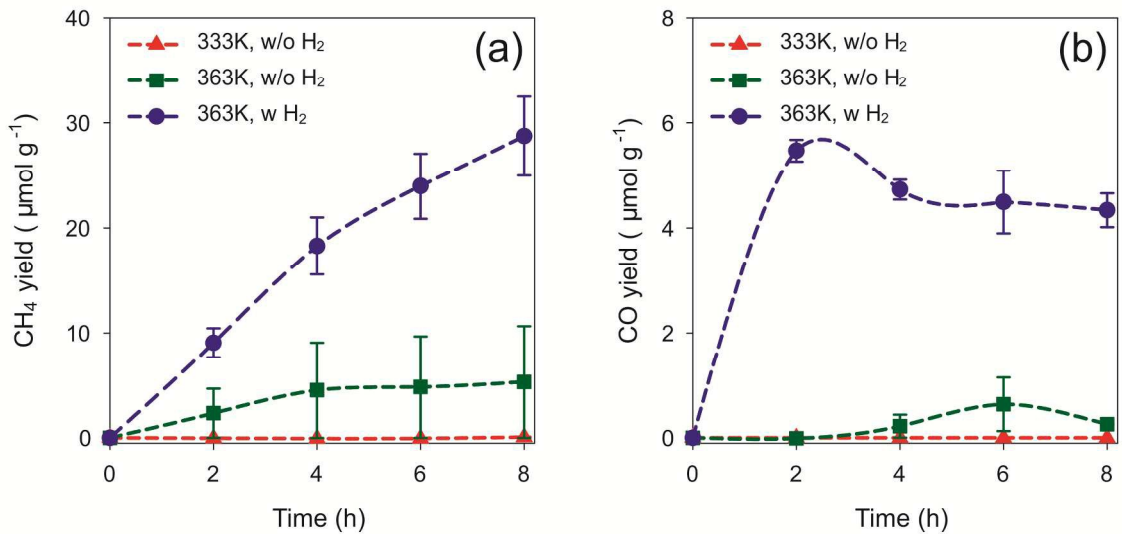


Figure 8. Reaction time profiles of the photocatalytic reduction of CO₂ with H₂O in the presence/absence of H₂ under different temperature to produce (a) CH₄ and (b) CO on 1%Cu/TiO₂ photocatalyst.

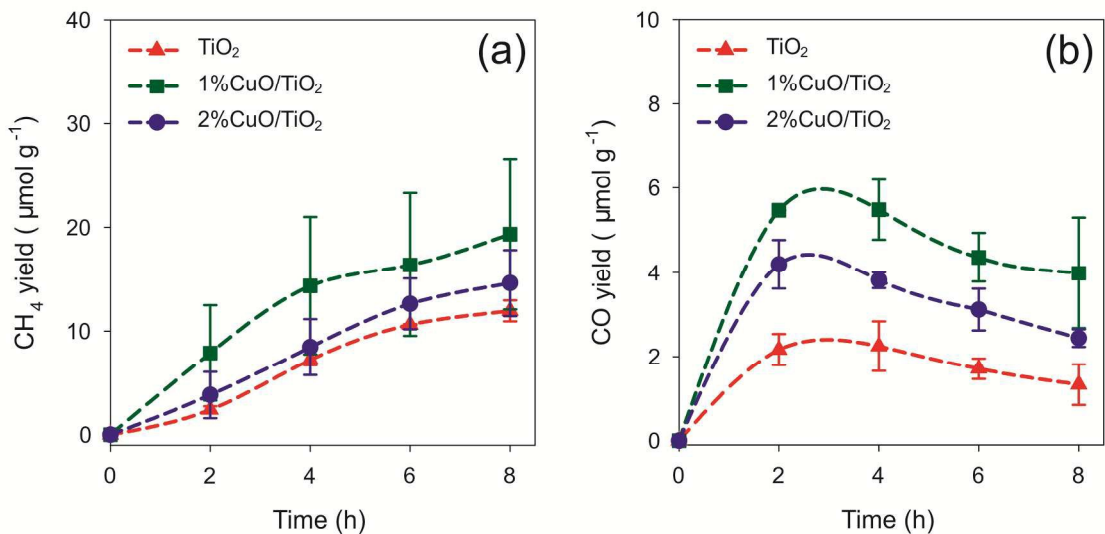


Figure 9. Reaction time profiles of the photocatalytic reduction of CO₂ with H₂O and H₂ to produce (a) CH₄ and (b) CO on different amount of CuO loaded TiO₂ photocatalysts.

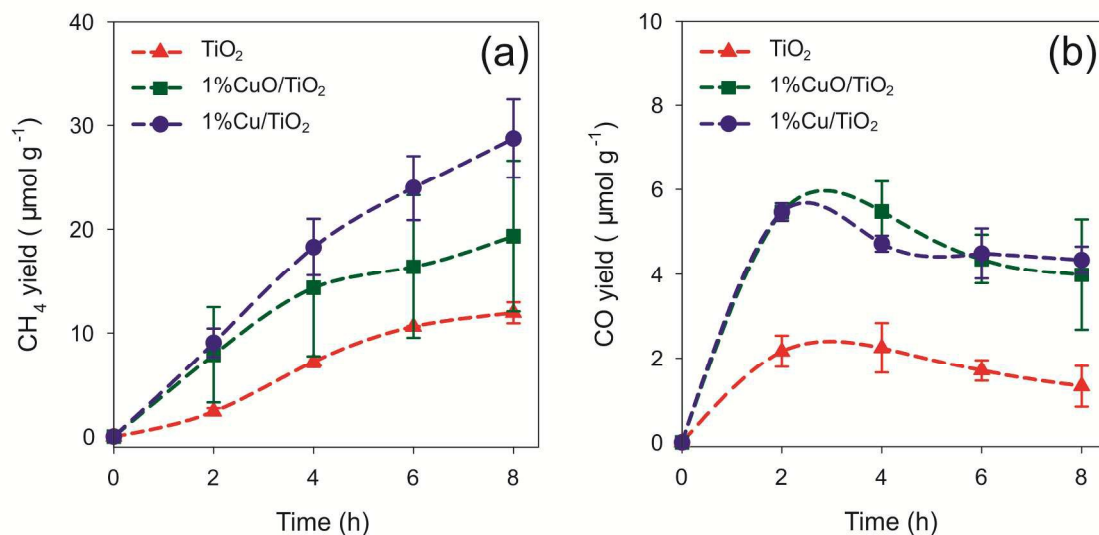


Figure 10. Reaction time profiles of the photocatalytic reduction of CO₂ with H₂O and H₂ to produce (a) CH₄ and (b) CO on different Cu oxidation state photocatalysts.

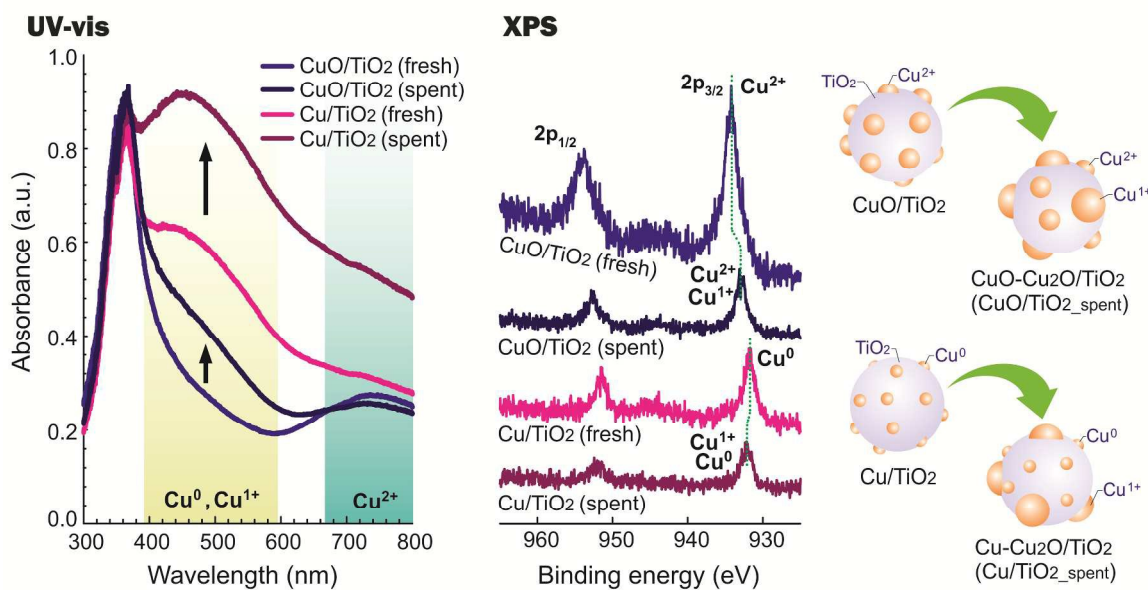


Figure 11. The transition of the nature of Cu species during the photoreaction.

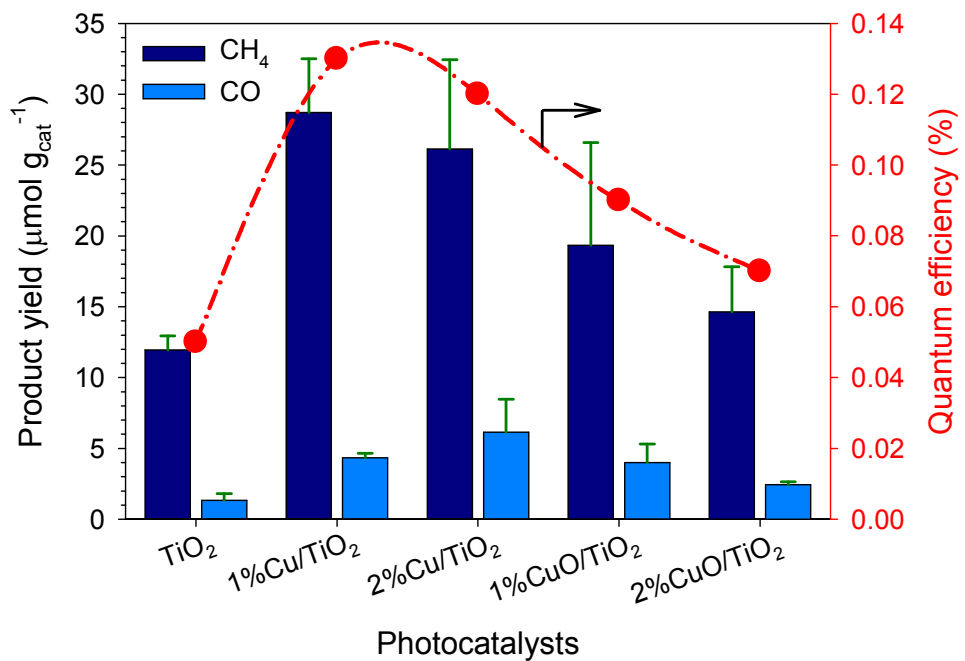


Figure 12. Performance comparison of the products yields (after 8 h in reaction) and the quantum efficiency on different photocatalysts.